Opto-electro-fluidics and tip coax conical surface plasmons

Touvia Miloh*
School of Mechanical Engineering, University of Tel-Aviv, Tel-Aviv 69978, Israel
(Received 20 January 2016; published 23 August 2016)

The concept of electromagnetic energy enhancement and nanofocusing phenomena near the tip of a metaconical conducting tip by means of a surface plasmon-polaritons mechanism is discussed theoretically. In particular, we consider conical metallic structures with small apex angles and derive the corresponding dispersion relation under optimal (maximal field enhancement) operating conditions. It is demonstrated analytically that the aforementioned conditions can induce large dielectrophoretic forces near the conical tip, which can be harnessed for sorting and controlling nanoparticles in a manner similar to optical tweezers. Similarly, by considering Joule heating effects in the metal and heat conduction in the surrounding solute, it is shown that a considerable (dc) flow convection and mixing can be generated in the aqueous phase near the tip by such ac incited optical means (including common low-input lasers operating in the visible and near-infrared spectrum ranges). Analytic near-field expressions are also obtained for the opto-electro-thermo-induced flow and vorticity distributions in the electrolyte exhibiting a singular behavior near the rounded tip. Using a coax conical metastructure composed of two noble metals, surface-plasmon field enhancement is a technique for the optimal manipulation of dielectric and polarizable nanoparticles as well as for inducing indirect mixing in the liquid around the tip by generating microvortices.

DOI: 10.1103/PhysRevFluids.1.044105

I. INTRODUCTION

Current nanotechnologies employ several noninvasive means (e.g., mechanical, electrical, magnetic, and optical) for manipulating and sorting nanoparticles and biomolecules, as well as for introducing indirect mixing and pumping effects in nanofluids [1–3]. Among the more recent promising and versatile techniques often used in biological applications (e.g., micromanipulation of DNA [4–6]), we call attention to the so-called optical methods, which are based on using standard light or laser sources (from the visible to the near-infrared spectrum range) that can be easily controlled by adjusting light intensity [7]. Since the dielectrophoretic (DEP) force exerted on a freely suspended dielectric or conducting nanoparticle (NP) depends on the gradient of the modulus of the electric field, the most common optical manipulation technique is based on using optical-electric tweezers (OET) that utilize radiation pressure from photons, which was first suggested by Ashkin [8]. Practically speaking, the main drawback of OET relates to the fact that the relatively high optical intensities required to generate considerable DEP effects can also lead to excessive Joule heating effects causing damage of biological particles as well as overheating and possible boiling in the electrolyte.

A popular approach towards obtaining more efficient delivery and enhanced optical energy at the subwavelength (nano) range relies on using certain waveguides and guiding nanofocusing structures, such as tapered metallic nanorods [9–13]. Indeed, large electromagnetic (EM) energy enhancement (by three to four orders of magnitude) and a strong focusing near the tip can be achieved under special surface-plasmon-polariton (SPP) or converging-polariton-resonant (CPR) conditions, where EM waves are formed at the interface between a metal and dielectric due to near-surface collective oscillations of electron gases [14–16]. Diffraction limit theory implies that it is generally difficult to concentrate electromagnetic wave energy in the dielectric material down to scales that are smaller than the ambient wavelength (i.e., several hundredths of a nanometer). However, this

*miloh@eng.tau.ac.il

restriction can be adverted at subwavelength distances from the surface of a superconductor by means of SPP enhancement when using specific materials such as noble metals (e.g., gold or silver). These metals are characterized by a frequency-dependent complex permittivity, such that for regular optical frequencies (namely, wavelengths below 1000 nm), its real part is usually negative and the corresponding imaginary part is positive [17] (equivalent to small dipole antenna in RF).

As for the shape of the regular or metastructure (two or three dimensional) that can sustain EM nanofocusing near geometrical singularities [18] (tips or corners) via SPP modes, we choose to consider here the particular geometry of a slender (small apex angle) tapering axisymmetric metal cone that yields high field intensity around the tip. Laser axial irradiation of the cone produces an oscillating evanescent standing wave (surface plasmon) on the metal-dielectric interface with wavelengths near the tip shorter than the wavelength of the illuminating light. Note that with current technologies it is possible to fabricate sharp conical tips as small as 5–10 nm. Theoretical aspects of the optical problem related to electric-field focusing and enhancement near a conical tip (singularity) through the excitation of SPP have been extensively discussed in the literature over the past decade under various approximations (see, for example, [19–33]). Most of these EM studies (except [33]) are based on using slender-body and WKB-type approaches and mainly consider homogeneous (single-metal) conical metallic nanostructures, with the exception of [19,24,29,30,32], which examine coax conical metastructures composed of two materials of different dielectric properties in perfect bonding.

The nanocone is surrounded by an otherwise unbounded fluid [deionized (DI) water or conducting electrolyte] and is assumed to be exposed to a monochromatic azimuthal transverse magnetic (TM) plane wave field propagating along the cone axis, illuminated by a common low-intensity (e.g., HeNe) laser operating in the visible or near-infrared range (i.e., vacuum wavelengths 500–2000 nm). The transverse operating mode can be attained by employing regular lasers with the aid of special masks and polarization converters that realize circular vectorial beams that are either (electric-field) azimuthally or radially polarized. Our rather ambitious task in the present study is to analytically consider the combined plasmo-thermo-fluidic [34–38] problem that merges light and fluids at nanoscales (see, for example, the recent review [39]), by using a coax nanocone incited by a regular laser operating under optimal (most singular) SPP or CPR conditions. Here we consider such a combined nonlinear problem (involving electromagnetism, heat transfer, and fluid dynamics) analytically. In particular, we attempt to analyze theoretically the corresponding opto-dielectro-phoretic effect and discuss the feasibility of using such a technique for manipulating freely suspended metallic and biological NP lying in a solute near the tip of a metallic nanocone optically excited by SPP [33,40]. It is also worth mentioning that similar techniques, based on using strongly localized SPP modes, have been successfully used for Raman spectroscopy combined with atomic force microscope applications [10,41]. In addition, by incorporating Joule heating effects and plasmon-incited convection in the aqueous phase, we try to estimate the dc component of the induced velocity and vorticity fields (related to fluid mixing) near the conical tip.

The corresponding electro-osmotic-induced dc fluid mixing phenomena observed at low frequencies well below the Maxwell-Wagner (megahertz) limit and the appearance of strong vortices near geometric (mainly two-dimensional) singularities (such as tips or corners) of polarizable shapes have been theoretically and experimentally demonstrated before (see, for example, [42–45]). However, it is well understood that a steady (dc) fluid mixing cannot be incited by electro-osmosis for optical (terahertz) frequencies, since under such relatively high frequencies the electric double layer does not have enough time to charge itself during a single period. We present here the feasibility and a theoretical study of the formation of steady plasmonic tip-induced nanovortices and flow mixing near a three-dimensional singularity (apex of a slender coax cone) in the optical frequency range. Such a plasmofluidic-based method can be effectively used for sorting, controlling, and manipulating (including trapping and levitation) of freely suspended NP and inciting fluid mixing on a nanoscale.

The structure of the paper is as follows. In Sec. II we discuss analytically the case of a transverse magnetic (TM) monochromatic wave field induced by a regular light or laser source in the presence of a metametallic nanocone composed of two noble metals. We first resolve the Maxwell equations in the different phases (metal and liquid) for the various scattering magnetic- and electric-field components

under the proper EM interface matching conditions. By employing conical (Mehler) functions [46–50] and using asymptotic expansions that prevail near the tip of a slender (small apex angle) conical structure, we obtain a dispersion relation for the resonant SPP conditions that determine the pertinent eigenvalue (generally complex) of the conical functions for the particular two-metal coax cone arrangement. It is then shown that a maximal (optimal) electric-field enhancement at the tip is obtained when the imaginary part of the eigenvalue vanishes, which corresponds here to the most singular solution with respect to the radial distance from the tip. As demonstrated in the following, this condition can be attained, however, only by using a special metastructure composed, for example, of two distinct coax noble metals (e.g., gold and silver) of different permittivity in perfect contact.

We indicate in Sec. III how such large electric-field gradients, induced in the aqueous phase around the rounded tip by common (low-input) lasers, can indeed be harnessed for generating relatively large DEP forces that can be used for steering and controlling free NPs. An interesting question then arises whether such a high-frequency light source that interacts resonantly with a rather thin conducting cone under optimal SPP conditions can indeed generate a steady (dc) electrothermal (ET) flow in the solute near the tip. This point is further discussed in Sec. IV, where we demonstrate that such a plasmonic-induced ET flow can be generated by means of thermal convection near the rounded tip as a result of Joule heating effects inside the cone. We provide an approximate near-field simplified solution for the temperature field within the narrow nanocone under optimal SPP or CPR conditions as well as obtaining an estimate for the radial temperature gradient in the solute near the tip. Finally, by including the dielectric force density term (assuming a temperature dependence of solute permittivity) in the momentum (Stokes) equation in the aqueous phase, we derive analytic expressions for both the plasmonic-induced axisymmetric steady velocity (stream function) and the azimuthal (toroidal) vorticity fields generated near the rounded conical tip. We conclude with a short summary and discussion in Sec V.

II. DISPERSION RELATIONS FOR COAX CONICAL PLASMONICS

We consider a semi-infinite coaxial straight nanocone consisting of two noble materials (perfect contact) of distinct complex permittivity and permeability denoted by (ε_1,μ_1) and (ε_2,μ_2) with the corresponding conical apex angles designated by 2α and 2β (see Fig. 1) such that $\beta \geqslant \alpha$. The conical structure is exposed to an axial time-harmonic (monochromatic) azimuthal TM field of a given frequency ω, where the only nonvanishing components of the induced EM fields are

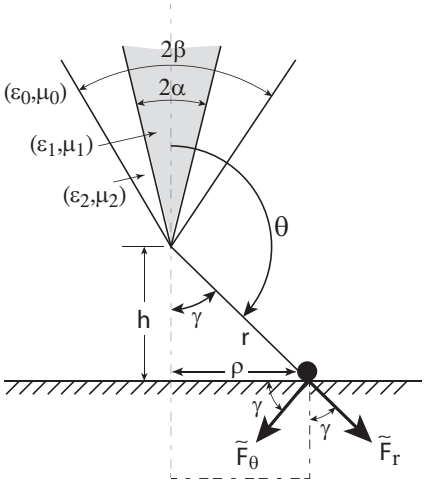

FIG. 1. Coax cone and substrate definition sketch.

$\vec{H}(r,\theta,\varphi;t) = \mathrm{Re}\{(0,0,H_\varphi(r,\theta,0))e^{-i\omega t}\}$ and $\vec{E}(r,\theta,\varphi;t) = \mathrm{Re}\{(E_r(r,\theta,0),E_\theta(r,\theta,0),0)e^{-i\omega t}\}$. This particular optical excitation is selected in order to render an analytical solution for the transverse electromagnetic (TM) diffracted wave field. Here t denotes time and (r,θ,φ) represent a spherical coordinate system centered on the tip of the cone such that $\theta = 0$ coincides with the cone axis (Fig. 1). The magnetic- and electric-field vectors are represented, respectively, by $\vec{H}$ and $\vec{E}$, where ω denotes the frequency (invariant) of the light source (visible to near-infrared range). The cone is surrounded by a fluid medium (air, water, or electrolyte) with dielectric permittivity and permeability denoted by (ε_0,μ_0).

A separable eigensolution of the Helmholtz equation for the azimuthal magnetic scattering wave component (exhibiting a singularity near the tip as $r \to 0$) can be obtained from resolving the Maxwell equations within each conical region in the following form [49–51]:

$$H_\varphi^{(j)}(r,\theta,0) \sim \frac{J_{i\nu}(k_j r)}{r^{1/2}} P^1_{-1/2+i\nu}(\pm\cos\theta), \tag{1}$$

where $k_j^2 = \omega^2\mu_j\varepsilon_j$ and the indices $j = 1,2$ correspond to the two material domains in the coaxial conical structure (Fig. 1). Here $J_{i\nu}(k_j r)$ denotes the common Bessel function of order $i\nu$ (ν represents the eigenvalue that is generally a complex parameter to be determined from the jump conditions prevailing across the material interfaces) and

$$P^1_{-1/2+i\nu}(\pm\cos\theta) = \frac{d}{d\theta} P_{-1/2+i\nu}(\pm\cos\theta) = P^1_{-1/2-i\nu}(\pm\cos\theta), \tag{2}$$

where the conical functions $P_{-1/2+i\nu}(\pm\cos\theta)$ represent the Legendre polynomials (see [46–51]) of complex order $(-1/2 + i\nu)$ with argument $\pm\cos\theta$. Note, however, that $P_{-1/2+i\nu}(-\cos\theta)$ is unbounded inside the cone around the axis $\theta = 0$, whereas $P_{-1/2+i\nu}(\cos\theta)$ is singular on the axis of symmetry outside the cone (i.e., near $\theta = \pi$). Thus, the solution of $H_\phi^{(1)}(r,\theta,0)$ should depend only on $P^1_{-1/2+i\nu}(\cos\theta)$, whereas (as shown in the following) $H_\phi^{(2)}(r,\theta,0)$ is determined by both $P^1_{-1/2+i\nu}(\pm\cos\theta)$.

According to Maxwell's equations, the tip singularities of the magnetic and electric fields near the cone apex ($r \to 0$) are $\frac{J_{i\nu}(k_j r)}{(k_j)^{i\nu} r^{1/2}} \to r^{-1/2+i\nu}$ and $\frac{J_{i\nu}(k_j r)}{(k_j)^{i\nu} r^{3/2}} \to r^{-3/2+i\nu}$, respectively. Furthermore, since the EM energy must be finite at the tip, it can be shown [see the discussion in Ref. [49] (p. 89) and [52]] that the most singular solution (i.e., maximum plasmonic resonance) with respect to the radial distance from the tip is obtained for real values of the eigenvalue ν, where $J_{i\nu}(z)$ can be expanded around the origin as

$$J_{i\nu}(z) = \left(\frac{1}{2}z\right)^{i\nu} \sum_{m=0}^{\infty} \frac{\left(-\frac{1}{2}z^2\right)^m}{m!\Gamma(1+m+i\nu)}. \tag{3}$$

It is important to note that as long as ν is real the conical (Mehler) function $P^1_{-1/2+i\nu}(\pm\cos\theta)$ is also real [46,47]. In addition, since we require the solution to be symmetric with respect to $\pm\nu$ (ν is real); one can express the solution for the two magnetic field components within the coax cone, as

$$\begin{aligned} H_\varphi^{(1)}(r,\theta,0) &= \frac{A_1}{r^{1/2}} \frac{J_{i\nu}(k_1 r)}{(k_1)^{i\nu}} P^1_{-1/2+i\nu}(\cos\theta), \quad \alpha \geqslant \theta \geqslant 0 \\ H_\varphi^{(2)}(r,\theta,0) &= \frac{1}{r^{1/2}} \frac{J_{i\nu}(k_2 r)}{(k_2)^{i\nu}} \left[A_2 P^1_{-1/2+i\nu}(\cos\theta) + A_3 P^1_{-1/2+i\nu}(-\cos\theta)\right], \quad \beta \geqslant \theta \geqslant \alpha \end{aligned} \tag{4}$$

where A_1, A_2, and A_3 are all amplitude-related coefficients depending on irradiation to be determined. The magnetic field in the aqueous phase exterior to the cone of amplitude A_4 can be expressed accordingly as

$$H_\varphi^{(0)}(r,\theta,0) = \frac{A_4}{r^{1/2}} \frac{J_{i\nu}(k_0 r)}{(k_0)^{i\nu}} P^1_{-1/2+i\nu}(-\cos\theta), \quad \pi \geqslant \theta \geqslant \beta \tag{5}$$

where $k_0^2 = \omega^2 \mu_0 \varepsilon_0$. Finally, according to Maxwell's equations, the two components of the electric field within each domain can be written by virtue of (4) for $j = 0,1,2$ as

$$E_r^{(j)}(r,\theta,0) = -\frac{1}{i\omega\varepsilon_j}\frac{1}{r\sin\theta}\frac{\partial}{\partial\theta}\big[\sin\theta H_\varphi^{(1)}(r,\theta,0)\big], \quad E_\theta^{(j)}(r,\theta,0) = \frac{1}{i\omega\varepsilon_j}\frac{1}{r}\frac{\partial}{\partial r}\big[r H_\varphi^{(1)}(r,\theta,0)\big]. \quad (6)$$

The explicit solution for the EM field within the coaxial cone and the surrounding fluid medium contain four unknown (generally complex) coefficients A_1, A_2, A_3, and A_4 and one real (eigenvalue) parameter v. In order to determine these coefficients we use the common EM interface boundary conditions, which imply that the azimuthal magnetic- and tangential electric-field components are continuous across the bounding interfaces on $\theta = \alpha,\beta$ and so are the corresponding normal electric inductions $\varepsilon_i E_\theta^{(i)}$. In order to obtain the dispersion relation we have ignored contributions from surface charges and surface currents on the material interfaces [51]. Moreover, in the following analysis we look for local singular solutions in the vicinity of the tip where $r \to 0$, by applying the appropriate asymptotic expansions of the Bessel function (3). Thus, near the conical tip, one gets the following linear homogeneous system of four equations for the unknown coefficients A_1, A_2, A_3, and A_4:

$$A_1 P^1_{-1/2+iv}(\cos\alpha) = A_2 P^1_{-1/2+iv}(\cos\alpha) + A_3 P^1_{-1/2+iv}(-\cos\alpha), \quad (7a)$$

$$A_2 P^1_{-1/2+iv}(\cos\beta) + A_3 P^1_{-1/2+iv}(-\cos\beta) = A_4 P^1_{-1/2+iv}(-\cos\beta), \quad (7b)$$

$$\frac{A_1}{\varepsilon_1} P_{-1/2+iv}(\cos\alpha) = \frac{A_2}{\varepsilon_2} P_{-1/2+iv}(\cos\alpha) + \frac{A_3}{\varepsilon_2} P_{-1/2+iv}(-\cos\alpha) \quad (7c)$$

$$\frac{A_2}{\varepsilon_2} P_{-1/2+iv}(\cos\beta) + \frac{A_3}{\varepsilon_2} P_{-1/2+iv}(-\cos\beta) = \frac{A_4}{\varepsilon_0} P_{-1/2+iv}(-\cos\beta). \quad (7d)$$

Equations (7a) and (7b) render the continuity of $H_\varphi(r,\theta,0)$ on the surfaces $\theta = \alpha$ and $\theta = \beta$, respectively, and Eqs. (7c) and (7d) the continuity of $\varepsilon E_r(r,\theta,0)$ on the same interfaces. In deriving Eq. (7) we have used the following expression for the radial component of the electric field obtained from Eqs. (4) and (5) and the governing differential equation of the Legendre polynomials [47]:

$$E_r^{(1)}(r,\theta,0) = \frac{A_1}{\omega\varepsilon_1}\frac{v^2+1/4}{r^{3/2}}\left(\frac{iJ_{iv}(k_1 r)}{(k_1)^{iv}}\right)P_{-1/2+iv}(\cos\theta), \quad \alpha \geqslant \theta \geqslant 0 \quad (8a)$$

$$E_r^{(2)}(r,\theta,0) = \frac{v^2+1/4}{\omega\varepsilon_2 r^{3/2}}\left(\frac{iJ_{iv}(k_2 r)}{(k_2)^{iv}}\right)[A_2 P_{-1/2+iv}(\cos\theta) + A_3 P_{-1/2+iv}(-\cos\theta)], \quad \beta \geqslant \theta \geqslant \alpha. \quad (8b)$$

Explicit expressions for the four coefficients A_j (denoting the amplitudes of the electric field in the different media) can be explicitly found in terms of the geometric coax angles (α,β) and dielectric parameters $(\varepsilon_0,\varepsilon_1,\varepsilon_2)$. It is however noted that, under the above CPR conditions [33] (holding especially for a small cone opening angle), the scattering electric field around the tip of the metallic cone is usually much larger (up to a few orders of magnitude) due to the $r^{-3/2}$-type singularity compared to the exterior (irradiation) incident field.

Applying next the solvability conditions for the linear homogeneous system (7) then renders the dispersion relationship relating the eigenvalue v to the problem parameters (i.e., cone angles and permittivities) that control the CPR conditions prevailing near the tip of the coaxial cone:

$$\frac{P_{-1/2+iv}(-\cos\beta)P^1_{-1/2+iv}(\cos\alpha)}{P_{-1/2+iv}(\cos\beta)P^1_{-1/2+iv}(-\cos\alpha)}\left(\frac{\varepsilon_2}{\varepsilon_0}-1\right)\left(\frac{\varepsilon_2}{\varepsilon_1}-1\right)$$
$$= \left[1 - \frac{\varepsilon_2}{\varepsilon_0}\frac{P_{-1/2+iv}(-\cos\beta)P^1_{-1/2+iv}(\cos\beta)}{P_{-1/2+iv}(\cos\beta)P^1_{-1/2+iv}(-\cos\beta)}\right]\left[\frac{P_{-1/2+iv}(-\cos\alpha)P^1_{-1/2+iv}(\cos\alpha)}{P_{-1/2+iv}(\cos\alpha)P^1_{-1/2+iv}(-\cos\alpha)} - \frac{\varepsilon_2}{\varepsilon_1}\right]. \quad (9)$$

Equation (9) determines the relations between the two conical apex angles α,β and the real (yet unknown) eigenvalue υ (corresponding to the most singular case) with the various complex permittivities $\varepsilon_1,\varepsilon_2$ of the coax cone and fluid ε_0. Under these conditions, one generally obtains an optimal plasmonic resonance condition (i.e., maximum field enhancement near the tip). The above transcendental relation (9) can be further simplified by recalling that the various Legendre polynomials of complex order $P_{-1/2+i\upsilon}(\pm\cos\theta)$ are real functions for real υ. Furthermore, since the opening angles for typical slender nanocones can be considered small (i.e., $\alpha,\beta \ll 1$), one can use the following leading-order asymptotic expansion for the conical Mehler functions that hold for $\theta \to 0$ (see, for example, Ref. [49], p. 76):

$$P_{-1/2+i\upsilon}(\cos\theta) \sim 1, \quad P_{-1/2+i\upsilon}(-\cos\theta) \sim -\frac{2}{\pi}\cosh(\upsilon\pi)\ln\frac{\theta}{2},$$
$$P^1_{-1/2+i\upsilon}(\cos\theta) \sim \frac{(\upsilon^2+1/4)\theta}{2}, \quad P^1_{-1/2+i\upsilon}(-\cos\theta) \sim -\frac{2}{\pi}\frac{\cosh(\upsilon\pi)}{\theta}. \tag{10}$$

Thus, one gets, by substituting Eq. (10) in Eq. (9),

$$\lim_{\theta\to 0} \frac{P_{-1/2+i\upsilon}(-\cos\theta)P^1_{-1/2+i\upsilon}(\cos\theta)}{P_{-1/2+i\upsilon}(\cos\theta)P^1_{-1/2+i\upsilon}(-\cos\theta)} \sim \frac{1}{2}\left(\upsilon^2+\frac{1}{4}\right)\theta^2\ln\frac{\theta}{2}, \tag{11}$$

which is an asymptotically negative small quantity for $\theta \to 0$.

If one considers, for example, the case of a homogeneous nanocone (i.e., $\varepsilon_1 = \varepsilon_2$ and $\alpha = \beta$) as a limiting case, then the left-hand side of (9) vanishes and thus we get

$$\frac{\varepsilon_0}{\varepsilon_2} = \frac{P_{-1/2+i\upsilon}(-\cos\beta)P^1_{-1/2+i\upsilon}(\cos\beta)}{P_{-1/2+i\upsilon}(\cos\beta)P^1_{-1/2+i\upsilon}(-\cos\beta)}, \tag{12}$$

which is a known dispersion relation for a simple homogeneous cone (see, for example, [29,33]). Equation (12) is also in agreement with similar expressions obtained by using a different approach, such as that employed in Ref. [22], where the dispersion relation was derived in the context of superfocusing of plasmonic polaritons, or to those given in Refs. [53,54], which were deduced in connection with the classical Taylor cone hydrodynamic problem.

However, it is important to note here that a maximum plasmonic tip singularity, i.e., $r^{-1/2}$ and $r^{-3/2}$ for the magnetic and electric fields, respectively, can indeed be envisioned only for a purely real eigenvalue υ for which the right-hand side of Eq. (12) yields a negatively small (compared to unity) real value. This restriction implies that the ratio between the dielectric constants of the electrolyte and cone materials must be negative and real. In fact, this condition can be satisfied by most superconductors or noble metals in the optical range, wherein by using the common Drude-Sommerfeld frequency model it can be shown that while such materials have a pronounced positive imaginary part the real part is generally negative (see, for example, [55,56]).

Provided the permittivity ratio $\frac{\varepsilon_0}{\varepsilon_2}$ between the two phases can be approximately represented by a negative small real parameter (using, for example, the common undamped Drude model) and assuming that the nanocone opening angle β is also small ($\beta \ll 1$), then one can use Eqs. (10)–(12) to obtain the following explicit relation for the real eigenvalue υ in terms of the specific (negative) ratio $\frac{\varepsilon_0}{\varepsilon_2}$ and (positive) β:

$$\upsilon^2 + 1/4 = \frac{2\left(\frac{\varepsilon_0}{\varepsilon_2}\right)}{\beta^2\ln\beta/2} > 0, \tag{13}$$

which suggests that for a given (real) value of permittivity (fluid to metal) ratio and small β, the eigenvalue υ is real and of $O(1)$. However, for most practical cases involving real materials, the permittivity ratio $\varepsilon_0/\varepsilon_2$ is a complex quantity in the visible optical range. Thus, the general solution of Eq. (12) renders a complex eigenvalue ν, which implies that actually the tip singularity for the EM is less than $r^{-3/2}$ (corresponding to a suboptimal solution). Under such isotropic conditions

(namely, $\varepsilon_1 = \varepsilon_2$ and $\alpha = \beta$) one can verify from Eqs. (7) and (13) that indeed $A_3 = 0$ and

$$A_1 = A_2 = \frac{P^1_{-1/2+\nu}(-\cos\beta)}{P^1_{-1/2+i\nu}(\cos\beta)} = \frac{\varepsilon_2}{\varepsilon_0}\frac{P_{-1/2+i\nu}(-\cos\beta)}{P_{-1/2+i\nu}(\cos\beta)}. \tag{14}$$

The two coefficients A_1 and A_2 denote the amplification factors of the magnitude of the electric field within the homogeneous metallic cone with respect to the externally applied field of unit amplitude. Consider, for example, a homogeneous cone with a small opening angel of $\beta = 3^\circ$ and $\nu = 1$, for which case Eq. (14) gives $A_1 = 4300$ (see also [7,12,13]) corresponding to CPR amplification by at least three orders of magnitude near the conical tip.

For a given choice of the two apex angles (α,β), an optimal (i.e., most singular) solution based on a real eigenvalue ν can be obtained by rearranging the coax dispersion relation (9) to explicitly express the desired permittivity ratio $\varepsilon_2/\varepsilon_1$ of the metacone in terms of the prescribed value of $\varepsilon_2/\varepsilon_0$, where all dielectric coefficients are taken as frequency-dependent complex parameters. Thus, for some specific ratios of the permittivity of the outer coax material ε_2 to that of the electrolyte ε_0, one can uniquely find a particular complex value for the permittivity ε_1 for the inner coax that satisfies the optimal SPP resonance conditions for the given ε_0 and ε_2. Moreover, we recall that in the optical (visible to near-infrared) range (typical frequencies of a few hundred terahertz), the ratio between the dielectric coefficient of a highly conducting material (such as gold) to that of vacuum (taken here as unity) is typically a complex number with a negative real part and a positive imaginary part, where the modulus of the real part is generally much larger compared to that of the imaginary part.

Let us consider, for example, the case of a common HeNe laser [i.e., wavelength of 633 nm (red)] and a golden single nanocone in vacuum, which implies that $\varepsilon_2/\varepsilon_0 = -11.44 + 1.12i$ (see [55]). To compare, the corresponding permittivity ratio at the same wavelength for silicon is given by [55] $18.0 + 0.32i$. The fact that the real part is positive explains why silicon, as opposed to noble metals such as gold or silver, is not generally used in CPR. By invoking Eqs. (9)–(11), Eq. (13) can be extended for a complex ratio $\varepsilon_0/\varepsilon_2$ and a coax conical metastructure. Thus, the real eigenvalue ν can be uniquely determined in terms of the cone angle β and complex permittivity ratios ($\varepsilon_0/\varepsilon_1$ and $\varepsilon_1/\varepsilon_2$) from the following relation:

$$\nu^2 + 1/4 = \frac{2}{\beta^2 \ln\beta/2}\left[\mathrm{Re}\left\{\frac{\varepsilon_0}{\varepsilon_2}\right\} - \mathrm{Im}\left\{\frac{\varepsilon_0}{\varepsilon_2}\right\}\frac{\mathrm{Re}\left\{\frac{\varepsilon_1}{\varepsilon_2} - 1\right\}}{\mathrm{Im}\left\{\frac{\varepsilon_1}{\varepsilon_2} - 1\right\}}\right]. \tag{15}$$

The full dispersion-type relation (9) will be used next to find both the specific permittivity ε_1 and the value of α that must be selected for the inner coax material in terms of the specified real and imaginary parts of $\varepsilon_0/\varepsilon_2$ and the particular size of the outer opening angle β.

Substituting Eqs. (10) and (11) in Eq. (9) renders, for $\alpha,\beta \ll 1$,

$$\begin{aligned}
A &\triangleq \frac{P_{-1/2+i\nu}(-\cos\alpha)P^1_{-1/2+i\nu}(\cos\alpha)}{P_{-1/2+i\nu}(\cos\alpha)P^1_{-1/2+i\nu}(-\cos\alpha)} = \frac{1}{2}\left(\nu^2 + \frac{1}{4}\right)\alpha^2 \ln\frac{\alpha}{2},\\
B &\triangleq \frac{P_{-1/2+i\nu}(-\cos\beta)P^1_{-1/2+i\nu}(\cos\beta)}{P_{-1/2+i\nu}(\cos\beta)P^1_{-1/2+i\nu}(-\cos\beta)} = \frac{1}{2}\left(\nu^2 + \frac{1}{4}\right)\beta^2 \ln\frac{\beta}{2},\\
C &\triangleq \frac{P_{-1/2+i\nu}(-\cos\beta)P^1_{-1/2+i\nu}(\cos\alpha)}{P_{-1/2+i\nu}(\cos\beta)P^1_{-1/2+i\nu}(-\cos\alpha)} = \frac{1}{2}\left(\nu^2 + \frac{1}{4}\right)\alpha\beta \ln\frac{\beta}{2}.
\end{aligned} \tag{16}$$

Thus, the coefficients A, B, and C, defined by the corresponding right-hand sides of Eq. (16) are all negative quantities such that $1 > |B| > |C| > |A|$. Substituting Eq. (16) into Eq. (9) finally leads, by virtue of Eq. (15), to the following missing expression for the opening angle α of the inner

coax cone in terms of the complex permittivity ratios:

$$\frac{\alpha}{\beta}=\left[\mathrm{Im}\left\{\frac{\varepsilon_1}{\varepsilon_2}-1\right\}\frac{\mathrm{Re}\left\{\frac{\varepsilon_0}{\varepsilon_2}\right\}}{\mathrm{Im}\left\{\frac{\varepsilon_0}{\varepsilon_2}\right\}}-\mathrm{Re}\left\{\frac{\varepsilon_1}{\varepsilon_2}-1\right\}\right]^{-1}<1. \tag{17}$$

Since for most noble metals operating in the optical range both $\mathrm{Re}\{\frac{\varepsilon_0}{\varepsilon_2}\}$ and $\mathrm{Im}\{\frac{\varepsilon_0}{\varepsilon_2}\}$ are generally negatively small (compared to unity) quantities [55,56], the restriction that the right-hand side of Eq. (17) must be positive and less then unity indicates that the numerical value of the complex permittivity ε_1 of the inner coax must satisfy both $\mathrm{Re}\{\frac{\varepsilon_1}{\varepsilon_2}-1\}<0$ and $\mathrm{Im}\{\frac{\varepsilon_1}{\varepsilon_2}-1\}>0$. As shown below, these two conditions can be easily attained by choosing a particular metamaterial geometrical arrangement. Again, let us consider for the purpose of illustration the case of a gold-silver coax cone combination in air that is illuminated by a low-input laser in the optical (red) range (wavelength of 620 nm) where $\varepsilon_1/\varepsilon_0=-9.97+0.822i$ (see gold in Table 3 in Ref. [56]) and $\varepsilon_2/\varepsilon_0=-17.4+2.26i$ (see silver in Table 5 in Ref. [56]). Thus, we find that $\mathrm{Re}\{\frac{\varepsilon_0}{\varepsilon_2}\}=-0.0565$ and $\mathrm{Im}\{\frac{\varepsilon_0}{\varepsilon_2}\}=-0.00734$. Furthermore, if we choose, for example, a conical coax with an exterior opening angle of $\beta=6^\circ$ ($\sim$0.1 rad) and recall that in the present case $\frac{\varepsilon_1}{\varepsilon_2}-1=-0.431+0.0267i$, then for a maximum (optimal) CPR condition, Eq. (15) gives $\nu\sim3.4$, which uniquely determines the sought eigenvalue. In addition, Eq. (17) yields $\alpha/\beta=0.636$, which implies that the inner angle of the coax should be around 4°.

It can be also demonstrated that a similar optimal CPR condition can be obtained in the infrared optical range using the same noble metals. Thus, for the corresponding (vacuum) wavelength of about 1240 nm (infrared), one gets [56] $\varepsilon_2/\varepsilon_0=-64.5+2.09i$ (see gold in Table 3 of [56]) and $\varepsilon_2/\varepsilon_0=-81.5+5.06i$ (see silver in Table 5 of [56]). Choosing, for example, the same conical opening angle $\beta=6^\circ$, Eq. (16) gives now $\nu=0.078$ and according to Eq. (17) $\alpha/\beta=0.58$. Finally, we note that if instead of vacuum the surrounding aqueous medium is DI water (i.e., optical refractive index of 1.33), the value of the eigenvalue under the same CPR operating conditions is $\nu=1.13$, while the ratio α/β remains unchanged.

III. OPTODIELECTROPHORESIS NEAR A CONICAL TIP

We have demonstrated in the previous section that under optimal SPP (or CPR) conditions, considerable gradients of the electric field can be generated near the tip of a coax cone with an $r^{-3/2}$-type singularity near the apex (origin). Thus, we find that around the conical tip $\nabla|\vec{E}^2|\sim o(1/r^4)$ as $r\to0$, where r denotes the radial distance from the tip (Fig. 1). Freely suspended uncharged NPs in the surrounding aqueous phase, which are exposed to such highly nonuniform electric fields induced by the laser beam, will experience a relatively large DEP gradient force (compared to diffusion [57]) as long as their typical size (radius of few tens of nanometers) is small compared with the characteristic optical wavelength (several hundred nanometers), in accordance with the Rayleigh scattering model. In the opposite limit, namely, when the particle size is large compared to the incident wavelength, the corresponding optical force can be readily found by employing, for example, ray optics arguments. The more complicated intermediate case, when the size of the particle and ambient wavelength are of the same order of magnitude, can be resolved by applying the classical Mie theory (see, for example, [52] and Mie's seminal paper [58] on light scattering).

The gradient (DEP) force exerted on a free spherical dielectric (polarized) particle of radius a under the Rayleigh limit can be simply represented by the common dipole model [1] (see Ref. [7], Sec. 13.6) as

$$\vec{F}=\pi a^3\varepsilon_m\mathrm{Re}\{K(\omega)\}\nabla|\vec{E}^2|, \tag{18}$$

where $\varepsilon_m=\varepsilon_0 n^2$ is the relative permittivity (dielectric constant) of the surrounding medium and n is the corresponding refractive index (i.e., $n=1$ for vacuum). The Clausius-Mossotti (CM) term in

Eq. (18) is defined for a spherical geometry by

$$K(\omega) = \frac{\varepsilon_p - \varepsilon_m}{\varepsilon_p + 2\varepsilon_m}, \tag{19}$$

where $\varepsilon_p(\omega)$ represents the frequency-dependent permittivity of the particle, which can be expressed according to the Drude-Sommerfeld model (ignoring for simplicity interband transitions [7]) as

$$\varepsilon_p(\omega) = \varepsilon_\infty - \frac{\omega_p^2}{\omega^2 + i\Gamma\omega}. \tag{20}$$

In Eq. (20) ε_∞ denotes the background permittivity, ω_p represents the plasma frequency, and Γ is the so-called damping constant, which is equal to the inverse of the relaxation time of the free-electron gas. For example, for Au NPs these coefficients are given following [17] by

$$\varepsilon_\infty = 9, \quad \omega_p = 1.36 \times 10^{16}\ \text{Hz}, \quad \Gamma = 10^{14}\ \text{Hz}. \tag{21}$$

A maximum value of $\text{Re}\{K(\omega)\}$ is obtained near the Frölich frequency where $\text{Re}\{\varepsilon_p\} + 2\varepsilon_m = 0$, which for isotropic Au NPs occurs at frequencies on the order of a few hundred terahertz corresponding to a vacuum wavelength of ~530 nm (visible optical range). For larger wavelengths, we note, however, that $\text{Re}\{K(\omega)\}$ is positive definite and is usually $O(1)$.

The modulus of the electric field can be written in terms of its radial E_r and angular E_θ components as

$$|\vec{E}^2| = E_r E_r^* + E_\theta E_\theta^*, \tag{22}$$

where the asterisk superscript denotes a complex conjugate. Thus, by substituting Eqs. (6) and (8) in Eq. (22) one gets, in the surrounding liquid phase ($2\pi > \theta > \beta$) around the conical tip,

$$|\vec{E}^2(r,\theta,0;\nu)| = \frac{\nu^2 + 1/4}{r^3}\left|\frac{A_1}{\omega\varepsilon_1(\omega)}\right|^2 \left\{(\nu^2 + 1/4)[P_{-1/2+i\nu}(-\cos\theta)]^2 + \left[P^1_{-1/2+i\nu}(-\cos\theta)\right]^2\right\}. \tag{23}$$

Following Eq. (18), the two components of the DEP force $(\tilde{F}_r, \tilde{F}_\theta)$ [normalized with respect to $\pi a^3 \text{Re}\{K(\omega)\}|\frac{A_1}{\omega\varepsilon_1(\omega)}|^2$], exhibit an r^{-4} singular behavior near the tip and are given by

$$\tilde{F}_r(r,\theta,0;\nu) = -\frac{3(\nu^2 + 1/4)}{r^4}\left\{(\nu^2 + 1/4)[P_{-1/2+i\nu}(-\cos\theta)]^2 + \left[P^1_{-1/2+i\nu}(-\cos\theta)\right]^2\right\}, \tag{24}$$

$$\tilde{F}_\theta(r,\theta,0;\nu) = \frac{2(\nu^2 + 1/4)}{r^4} P^1_{-1/2+i\nu}(-\cos\theta)\{2(\nu^2 + 1/4) \times P_{-1/2+i\nu}(-\cos\theta) - \cot\theta\, P^1_{-1/2+i\nu}(-\cos\theta)\}. \tag{25}$$

Since we are mainly interested in finding the DEP force exerted on a freely suspended NP near the axis of symmetry (i.e., in the direction of the laser beam) where $\theta \sim \pi$ (Fig. 1), one can apply the following asymptotic expansion (see Ref. [46], p. 337) for $\theta = \pi - \gamma$ and $\gamma \ll 1$:

$$\begin{aligned} P_{-1/2+i\nu}(-\cos\theta) &= P_{-1/2+i\nu}(\cos\gamma) \\ &= 1 + (\nu^2 + 1/4)\sin^2\frac{\gamma}{2} + \frac{1}{4}(\nu^2 + 1/4)(\nu^2 + 9/4)\sin^4\frac{\gamma}{2} + \cdots. \end{aligned} \tag{26}$$

Substituting the above in Eqs. (24) and (25) renders, for small values of γ (namely, near the cone axis),

$$\tilde{F}_r \sim -\frac{3(\nu^2 + 1/4)}{r^4} + o(\gamma^2), \tag{27}$$

$$\tilde{F}_\theta \sim -\frac{3(\nu^2 + 1/4)}{2r^4}\sin\gamma + o(\gamma^3). \tag{28}$$

Consider next a dielectric free NP lying at $(x,y,-z)$ on a nonconducting flat substrate placed at a distance $h=-z$ below the conical tip, where z denotes the axial direction (surfactants can be also added to the solute to prevent particle sticking with substrate). Thus, the horizontal displacement from the axis $\rho=(x^2+y^2)^{1/2}=(r^2-z^2)^{1/2}$ is given by $\rho=h\tan(\gamma)$, where (ρ,z) is a cylindrical system centered around the conical tip (see Fig. 1). The horizontal (ρ direction) component of the DEP force exerted on the particle and pointing towards the axis is then given by (26) and (27) as

$$\tilde{F}_\rho=\tilde{F}_\theta\cos\gamma-\tilde{F}_r\sin\gamma=\frac{3(\nu^2+1/4)}{r^4}\left[1-\frac{1}{2}(\nu^2+1/4)\right]\sin\gamma+o(\gamma^3). \tag{29}$$

Thus, one finds from Eq. (29) that for all real and positive eigenvalues satisfying $\nu>\nu^*$ (where $\nu^*=\sqrt{7}/2=1.323$), the NP always moves horizontally along the substrate away from the axis (in a manner similar to negative dielectrophoresis) towards regions of smaller gradients, whereas for $\nu<\nu^*$ the particle is attracted to the axis (positive dielectrophoresis) where the modulus of the electric-field gradient is maximum as long as $\mathrm{Re}\{K(\omega)\}>0$. The opposite is true (i.e., reverse directions) if the real part of the CM coefficient is negative. Furthermore, since $\sin\gamma=\rho/r$, the attraction DEP force pulling the NP towards the axis of symmetry is linear in ρ (spring type) with a normalized eigenvalue-dependent spring constant (trap stiffness [7]) given explicitly by $(3/h^4)(\nu^2+1/4)(7/4-\nu^2)$. Note that a similar linear dependence of $\tilde{F}_\rho$ on ρ near the axis ($z\sim r$) is given in Eq. (13.60) of Ref. [7], however with a different tip singularity, namely, (ρ/r^6) instead of (ρ/r^5). The reason for this discrepancy is based on the far-field crude model of a point axial dipole placed at the tip used in Ref. [7] under the long-wave (Laplace) approximation. It is claimed that the present near-field analysis is exact in the sense that the scattering electric field near the conical tip (satisfying the Helmholtz equation) is determined analytically in terms of cone geometry and optical parameters.

From the physical point of view, we find that the DEP response in our conical SPP case is similar in many respects to the well-known trapping phenomena in optical tweezers and localized SPP resonances [8,39,40,59–67] and thus can be accordingly used for sorting and manipulating dielectric and conducting NPs by means of low-input lasers. It is also important to note that the trap $\rho=0$ on the axis of the substrate is a stable (equilibrium or fixed) point. Stability aspects of trapping phenomena can be also discussed in terms of the trapping potential function [60], which is generally normalized by the laser illumination intensity and the thermal energy k_BT (k_B is the Boltzmann constant and T the temperature). It was demonstrated, for example, by [66], that a potential well's depth of at least $10k_BT$ W^{-1} is sufficient to guarantee stable trapping in the sense that it overcomes its thermal energy and the ambient random fluid Brownian motion.

In addition to the above specific DEP-induced horizontal motion, the NP will also experience a vertical (levitation) force that increases with decreasing ρ (horizontal displacement). For example, if we denote the normalized weight (including buoyancy) of the particle by $\tilde{W}_p$, it will be practically lifted from the substrate due to the vertical component of the DEP force providing [recalling that both $\tilde{F}_r$ and $\tilde{F}_\theta$ in Eqs. (27) and (28) are negative] that

$$-(\tilde{F}_r\cos\gamma+\tilde{F}_\theta\sin\gamma)>\tilde{W}_p, \tag{30}$$

where $\gamma=\tan^{-1}(\rho/h)$. Thus, NPs that are trapped on the substrate near the axis will be levitated and move vertically towards the tip of the cone for clearance values of $h<h^*$ (a critical vertical distance of substrate from the origin), where the threshold distance h^* is simply given by

$$h^*(\nu)=\left(\frac{3}{\tilde{W}_p}\right)^{1/4}(\nu^2+1/4)^{1/2}. \tag{31}$$

It is finally remarked here that the critical spacing h^* of the substrate from the conical tip is only controlled by the positive SPP real eigenvalue ν, which in turn depends on the coax opening angles (α,β) and the permittivity ratios $(\frac{\varepsilon_1}{\varepsilon_0},\frac{\varepsilon_2}{\varepsilon_0})$ of the metamaterial through the explicit relations (15) and (17).

IV. PLASMONIC-INDUCED OPTOFLUIDIC NANOVORTICES

In this section we attempt to investigate analytically the problem of plasmonic-generated nanovortices (mixing) and controlled fluid pumping in the fluid near the tip of a conducting cone. It is well known that due to the relatively high laser operating frequencies (hundreds of terahertz in the visible range), electric charges cannot be induced in the solute since due to fast oscillations the Debye layer does not have sufficient time to charge itself [68] and thus electro-osmotic effects connected with the forming of an electric double layer on dielectric interfaces can be ignored. The contribution of the Coulomb force density (proportional to the induced electric charge) is practically null and thus can be neglected with respect to the dielectric body force, expressed in terms of the gradient of fluid permittivity ε_0 and the modulus squared of the scattered electric field induced near the conical tip. Under such high-frequency (optical) excitation, the electric body force acting on the electrolyte can be simply given by [69,70] $\vec{f}_e = -\frac{1}{2}\nabla\varepsilon_0|\vec{E}|^2$. Furthermore, assuming a continuum, Newtonian, and incompressible fluid, where inertia and convection can be neglected with respect to the viscous term, the nonhomogeneous (forced) Stokes equation can be written as

$$\eta\nabla^2\vec{V} = \nabla P + \tfrac{1}{4}\nabla\varepsilon_0|\vec{E}|^2, \quad \nabla\cdot\vec{V} = 0. \tag{32}$$

Here $\vec{V}$ and P represent the steady (dc) components of the SPP-induced fluid velocity and pressure, respectively, obtained by performing a time-averaging operation over a single period. The dynamic viscosity η is taken as constant and the permittivity of the electrolyte ε_0 is assumed to be a function of temperature such that for a typical DI water and aqueous NaCl solution $\frac{\partial}{\partial T}\ln\varepsilon_0(T) \sim -0.001\ \mathrm{K}^{-1}$, where T is the temperature and K denotes Kelvin degrees [69]. Thus, if one considers electrothermal effects that are generated, for example, by (relatively small) temperature gradients created in the electrolyte near the tip, as a result of excessive (Joule) heating effects of the tapered nanocone under CPR conditions, one can practically assume that $\nabla\varepsilon_0$ is proportional to ∇T.

Our next task is to find the plasmonic-induced temperature field in the electrolyte. In typical thermoplasmonic situations (see, for example, [71–76]), involving nanostructures composed of noble metals in a liquid phase, one must consider the temperature rise (Joule heating) in the conductor due to the large enhancement of the electric field around the tip (corner) under optimal resonant SPP situations. In particular, for a slender (narrow) conical structure with a small and smooth tapering angle towards a rounded conical tip of the order of few nanometers, the modulus of the electric field can grow (compared to irradiation) by two to three orders of magnitude [22,23,27,28,77,78]. If we further ignore heat convection versus heat diffusion, the dc temperature field can be expressed according to the common Joule model, by assuming that the heat generation (source) in the conductor is proportional to the square of the induced electric field times its electric conductivity (i.e., the imaginary part of the dielectric coefficient of the metal). Hence, when assuming a constant value for the thermal conductivity k_m for the metallic phase, the temperature field in the cone is governed by the following nonhomogeneous heat-conduction equation:

$$k_m\nabla^2 T_m = -\tfrac{1}{2}\sigma|\vec{E}|^2, \tag{33}$$

where T_m denotes the steady (dc) temperature in the metal and its electric conductivity (assumed constant) is simply given by $\sigma = \omega\mathrm{Im}(\varepsilon_1)$, where $\varepsilon_1(\omega)$, as before, represents the complex permittivity of the conical tip material and ω is the laser light frequency. Since the dielectric coefficient of the aqueous phase ε_0 is taken here as real (i.e., a negligibly small solute electric conductivity due to high optical frequency), the steady temperature distribution T_e in the surrounding liquid (ignoring natural convection) is simply assumed to be given by the Laplace equation $\nabla^2 T_e = 0$.

We can now proceed with the evaluation of the temperature distribution inside the conical nanostructure under continuous laser operation and CPR conditions (note that the case of a short-pulse laser is somewhat different [79]). It appears that no analytic solution for the temperature field near a conical tip for the thermoplasmonic problem has been reported in the literature, even for the case of a homogeneous cone (i.e., $\varepsilon_1 = \varepsilon_2$). Below, we provide an approximate solution for the temperature field within a semi-infinite conical domain, which fits some of the experimental observations and

indicates that the maximum temperature occurs around the tip and radially decays away from it along the cone axis [80–83]. Thus, by considering a homogeneous (gold) nanocone with a small opening angle $\alpha \ll 1$ and recalling that for a slender cone $0 \leqslant \theta \leqslant \alpha$, $P_{-1/2+i\upsilon}(\cos\theta) \to 1$ and $P^1_{-1/2+i\upsilon}(\cos\theta) \to 0$, the right-hand side of (33) together with (23) when θ is replaced by $\pi - \theta$ leads to

$$\nabla^2 T_m(r) = -\frac{q_0}{r^3}, \quad q_0 = \frac{\mathrm{Im}\{\varepsilon_1(\omega)\}(\upsilon^2 + 1/4)^2}{2k_m\omega}\left|\frac{A_1}{\varepsilon_1(\omega)}\right|^2. \tag{34}$$

Here q_0 denotes the total irradiation power absorbed by the conical tip and converted into heat and can be considered as a prescribed parameter. Following [72,84], the thermal conductivities of gold and silver can be taken as $k_{m(\mathrm{gold})} = 318$ nW/nmK and $k_{m(\mathrm{silver})} = 427$ nW/nmK. The total absorption power by the surface of a semisphere of radius r_0 replacing the conical apex can be calculated according to $q \sim 2\pi r_0^2 p$, where p denotes light irradiation. A typical value for the incident light intensity (irradiance) of a regular laser is [71,74,85] $p \sim 10^4$ W/cm^2 (the total power q, for example, of commercial Thor-Labs HeNe lasers varies between 0.8 and 23 W). However, as previously mentioned, under CPR conditions the enhancement in the electric field near the tip is usually larger by at least two to three orders of magnitude [84] and thus, for a typical tip radius of $r_0 \sim 10$ nm and modest amplification factor of 10^2, the absorption power at the tip vicinity can be as high as 10–100 μW (see, for example, [85–87]).

The Poisson equation (34) can be analytically solved for the radial temperature distribution in the metal phase within a very narrow nanocone $r \geqslant r_0$, $\theta \leqslant \alpha \ll 1$, providing we ignore the θ dependence due to cone slenderness and consider only radial temperature variations. Under this simplifying assumption, which prevails for a relatively thin tapering cone, the nonhomogeneous heat conduction equation can be solved exactly ($r^{-1}\log r$) and when combined with that of the homogeneous (Laplace) equation (r^{-1}) leads to

$$T_m(r) = \frac{q_0}{r}[1 + \log(r/r_0)] \quad \text{for } r \geqslant r_0. \tag{35}$$

Note that, based on physical arguments, the temperature field near the tip of a narrow cone (35) must be bounded. Thus, when looking for an approximate analytic solution, a zero-heat-flux condition is usually imposed on the rounded tip (see, for example, [88] and Ref. [89], Sec. 3-7), namely, $\frac{\partial T_m(r)}{\partial r} = -\frac{q_0}{r^2}\log(r/r_0) \to 0$ as $r \to r_0$, so as to get a tangible solution near the cone apex. The maximum temperature $\bar{T}_m = T_m(r_0) \sim \frac{q_0}{r_0}$ occurs near the conical tip ($r = r_0$) and radially decays along the cone axis away from the tip, whereas the maximum heat flux occurs a few radii below the tip (see [60,80,90–92]) as $\log(r/r_0) \sim 1$. Thus, for a conical tip with $r_0 \sim 10$ nm and local irradiation power of about 50 μW, the maximum temperature rise at the tip of the cone is approximately 15 °C (gold) and 12 °C (silver). Decreasing the tip radius by half (5 nm) increases the temperatures by a factor of 2.

The temperature distribution in the surrounding liquid phase $T_e(r,\theta)$ is governed by the Laplace equation (nonconducting solute) and can be obtained by applying the proper boundary conditions on the bounding interface. Enforcing the continuity conditions of both temperature ($\frac{\partial T_e}{\partial r} = \frac{\partial T_m}{\partial r}$) and normal heat flux ($k_e\frac{\partial T_e}{\partial \theta} = k_m\frac{\partial T_m}{\partial \theta} \to 0$) on the surface of the slender cone $\theta = \alpha \ll 1$ suggests that at least near the conical tip the radial heat flux prevails over the normal (to the surface) flux, since the thermal conductivity of the solute k_e is usually smaller by a few orders of magnitude [60,72] when compared against that of the metal. Thus, the dominant component of the SPP-induced temperature gradient in the solute near the conical apex is considered to be purely radial (similar to a point heat source of output q_0 located at the tip of the cone).

Having obtained an analytic expression for the temperature distribution in the liquid phase, our next task is to resolve the optofluidic problem governed by (32) and estimate the thermoplasmonic-induced velocities by the corresponding dielectric force density. Towards this goal, one can consider the solute permittivity to be temperature dependent $\varepsilon_0(T)$ and thus $\nabla\varepsilon_0(T) \sim K_e\bar{\varepsilon}_0\nabla T$, where $\bar{\varepsilon}_0$

represents the ambient (room temperature) value of the permittivity of the solute. A typical value for the coefficient K_e (say, for NaCl) is [69] -0.4% K^{-1}.

In order to eliminate the pressure term in Eq. (32) and reduce the vectorial momentum equation to a scalar one in terms of the Stokes stream function $\psi(r,\theta)$, we apply the curl operator to Eq. (32), which eventually leads to (see [93,94])

$$\Delta^2[\Delta^2\psi(r,\theta)] = -\frac{Ke\bar{\varepsilon}_0}{4\eta}\frac{dT_e}{dr}\sin\theta\frac{\partial|\vec{E}|^2}{\partial\theta}. \tag{36}$$

The second-order differential operator (not to be confused with the Laplacian ∇^2) on the left-hand side of Eq. (36) is defined as

$$\Delta^2 = \frac{\partial^2}{\partial r^2} + \frac{\sin\theta}{r^2}\frac{d}{d\theta}\left(\frac{1}{\sin\theta}\frac{d}{d\theta}\right). \tag{37}$$

In addition, we recall (following previous discussion) that the radial temperature gradient in the electrolyte near the rounded tip is approximately given by $\frac{dT_e}{dr} \sim -\frac{q_0}{k_m r^2}\log\frac{r}{r_0}$ and that the induced EM-field intensity $|\vec{E}|^2$ in the surrounding fluid medium is explicitly given in Eq. (23). Note also that by virtue of Eq. (2) one gets

$$\begin{aligned} r^3\frac{\partial|\vec{E}|^2}{\partial\theta} &= 2\left(\upsilon^2+\frac{1}{4}\right)P^1_{-1/2+i\upsilon}(-\cos\theta)\left|\frac{A_1}{\omega\varepsilon_1(\omega)}\right|^2 \\ &\quad\times\left\{\left(\upsilon^2+\frac{1}{4}\right)P_{-1/2+i\upsilon}(-\cos\theta)+\frac{d^2P_{-1/2+i\upsilon}(-\cos\theta)}{d\theta^2}\right\}. \end{aligned} \tag{38}$$

For the sake of obtaining an analytic solution for Eq. (36), we find, following Eq. (26), that near the laser beam axis ($\theta \sim \pi$), the term in curly parentheses in Eq. (38) is a slowly varying function of θ, which for, say, $\theta = \pi$ is simply equal to $\frac{3}{2}(\upsilon^2+\frac{1}{4})$. Thus, the right-hand side of Eq. (36), which determines the Stokes stream function, can be written as

$$\Delta^4\psi(r,\theta) = D\frac{\sin\theta P^1_{-1/2+i\upsilon}(-\cos\theta)\log(r/r_0)}{r^5}, \quad D = \frac{3K_e\bar{\varepsilon}_0 q_0}{4\eta k_m}\left|\frac{A_1}{\omega\varepsilon_1(\omega)}\right|^2\left(\upsilon^2+\frac{1}{4}\right)^2. \tag{39}$$

A particular solution of the above inhomogeneous fourth-order partial differential equation (PDE) (39) can be finally expressed in the following form:

$$\psi(r,\theta) = \frac{D\lambda_1}{r}[\log(r/r_0)+\lambda_2]\sin\theta P^1_{-1/2+i\upsilon}(-\cos\theta), \tag{40}$$

where D is considered prescribed in terms of problem parameters and the two additional parameters $\lambda_{1,2}(\upsilon)$ in Eq. (40) are defined as

$$\lambda_1 = [(\nu^2+1/4)+14(\nu^2+1/4)+24]^{-1}, \quad \lambda_2 = 10\lambda_1(\nu^2+21/4). \tag{41}$$

In order to verify that Eq. (40) is indeed a particular solution of Eq. (39), one can use the following relation for the conical functions (see, for example, Ref. [47], p. 444, or Ref. [48], p. 337):

$$\frac{1}{\sin\theta}\frac{d}{d\theta}\left[\sin\theta P^1_{-1/2+i\upsilon}(-\cos\theta)\right] = \left(\upsilon^2+\frac{1}{4}\right)P_{-1/2+i\upsilon}(-\cos\theta). \tag{42}$$

It is worth nothing that near the rounded conical tip ($r \sim r_0$), the logarithmic term in parentheses in Eq. (40) can be ignored with respect to the coefficient λ_2 defined in Eq. (41). Furthermore, in order to impose and satisfy the no-slip velocity condition on the surface of the cone $\theta = \alpha$, we note, following [93,94], that the corresponding solution of the homogeneous PDE, $\Delta^4\psi = 0$, exhibiting an r^{-1}-type singularity near the origin, can be simply written as $r^{-1}\sin\theta P^1_n(\cos\theta)$ for $n = 1,3$, where $P^1_n(\cos\theta) = \frac{d}{d\theta}P_n(\cos\theta)$ denotes the associated Legendre functions. Thus, the complete near-field

solution for the Stokes stream function, prevailing at the vicinity of the conical tip, can be written by adding these two homogeneous solutions to the inhomogeneous one given in Eq. (40), resulting in

$$\psi(r,\theta) \sim \frac{D\lambda_1\lambda \sin\theta}{r}\left[P^1_{-1/2+i\nu}(-\cos\theta) + C_1 P^1_1(\cos\theta) + C_3 P^1_3(\cos\theta)\right], \tag{43}$$

where the coefficients C_1 and C_3 in Eq. (43) are obtained by enforcing the common velocity no-slip conditions on the solid surface of the cone $\theta = \alpha$, namely, $\psi(r,\alpha) = \frac{\partial\psi}{\partial\theta}(r,\alpha) = 0$. These two boundary conditions together with $\psi(r,\pi) = 0$ explicitly ensure that the optoinduced fluid motion near the conical tip is purely circulatory with vanishing velocities away from it. The two unknown coefficients $C_{1,3}$ in Eq. (43) can be readily found by invoking the above no-slip boundary conditions on $\theta = \alpha$. Thus, by using the asymptotic leading-order expansions (10) for a slender cone ($\alpha \ll 1$), one gets

$$\begin{aligned} C_3 &= \frac{2P^1_{-1/2+i\nu}(-\cos\alpha)}{15\sin^3\alpha} - \frac{(\nu^2+1/4)P_{-1/2+i\nu}(-\cos\alpha)}{15\cos\alpha} = -\frac{4\cosh(\pi\nu)}{15\pi\sin^4\alpha} + o(\alpha^2\ln\alpha), \\ C_1 &= -\left(6 - \frac{15}{2}\sin^2\alpha\right)C_3 + \frac{P^1_{-1/2+i\nu}(-\cos\alpha)}{\sin\alpha} = \frac{8\cosh(\nu\pi)}{5\pi\sin^4\alpha} + O(\alpha^2\ln\alpha). \end{aligned} \tag{44}$$

The explicit expression (43) thus obtained for the Stokes stream function together with Eqs. (41)–(44) render the sought near-field solution for the complete OET problem governed by the nonhomogeneous equation (39). It also provides analytic expressions for the SPP-induced radial and angular (dc) velocity components in the aqueous phase near the rounded tip of an illuminated thin nanocone due to the dielectric force density given on the right-hand side of Eq. (32).

Our interest in the present study is connected, however, with the possibility of creating optoelectrically [71,95–97] induced vorticity-driven fluid mixing near a conical tip in an otherwise quiescent liquid. Thus, our next task is to determine the corresponding vorticity field that results from the axisymmetric flow pattern given by Eq. (43) which has only a single azimuthal component denoted by $\zeta_\varphi(r,\theta)$. It is also worth noting that this particular component can be directly obtained from the Stokes stream function (43) and the second-order partial operator Δ^2 defined in Eq. (37) (see, for example, [98,99]) as

$$\zeta_\varphi(r,\theta) = -\frac{\Delta^2\psi(r,\theta)}{r\sin\theta}. \tag{45}$$

Thus, following Eq. (42) we note that

$$\begin{aligned} \Delta^2\left(\frac{\sin\theta P^1_{-1/2+i\nu}(-\cos\theta)}{r}\right) &= \frac{\nu^2+\frac{9}{4}}{r^3}\sin\theta P^1_{-1/2+i\nu}(-\cos\theta), \\ \Delta^2\left(\frac{\sin\theta P^1_n(\cos\theta)}{r}\right) &= \frac{(n^2+n-2)\sin\theta P^1_n(\cos\theta)}{r^3}, \end{aligned} \tag{46}$$

which, when applied in conjunction with Eq. (43), finally renders the relatively simple expression

$$\zeta_\varphi(r,\theta) \sim -\frac{D\lambda_1\lambda_2}{r^4}\left[(\nu^2+9/4)P^1_{-1/2+i\nu}(-\cos\theta) + 10C_3P^1_3(\cos\theta)\right] \tag{47}$$

since the term proportional to C_1 in Eq. (43), representing a potential dipole, does not contribute to the vorticity by virtue of Eq. (46).

Closer scrutiny of Eq. (47) reveals that the maximum azimuthal vorticity is observed at $\theta \sim \alpha$, i.e., near the conical surface (similar to Prandtl's boundary layer theory). Furthermore, the vorticity field decays as r^{-4} away from the rounded tip and its amplitude is inversely proportional to the opening cone angle and varies like $(\sin\alpha)^{-3}$. Thus, considerable mixing is expected near the tip of a relatively slender (needle-type) coax cone under CPR conditions. Finally, for the purpose of illustration we also provide (see Fig. 2) some schematic normalized (with respect to $D\lambda_1\lambda_2C_1$) near-field polar plots

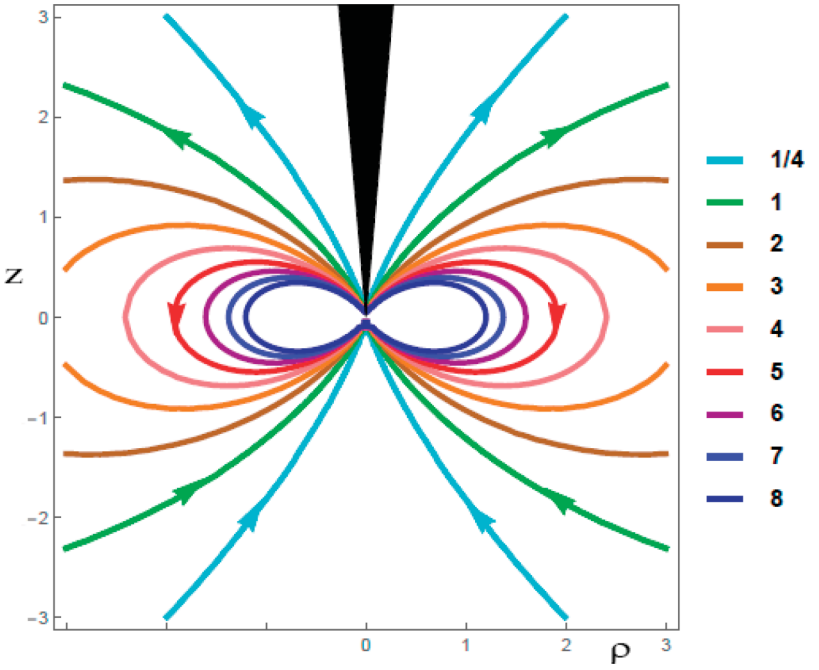

FIG. 2. Plot of Stokes streamlines following Eq. (43) (normalized with respect to $D\lambda_1\lambda_2 C_1$).

of typical streamlines according to Eq. (43). The velocity field exhibits an r^{-3}-type singularity and the radial component along the free beam axis ($\theta \sim \pi$) is directed towards the tip (sucking mode) and away from it along the conical surface (pumping mode). The presented numerical simulations

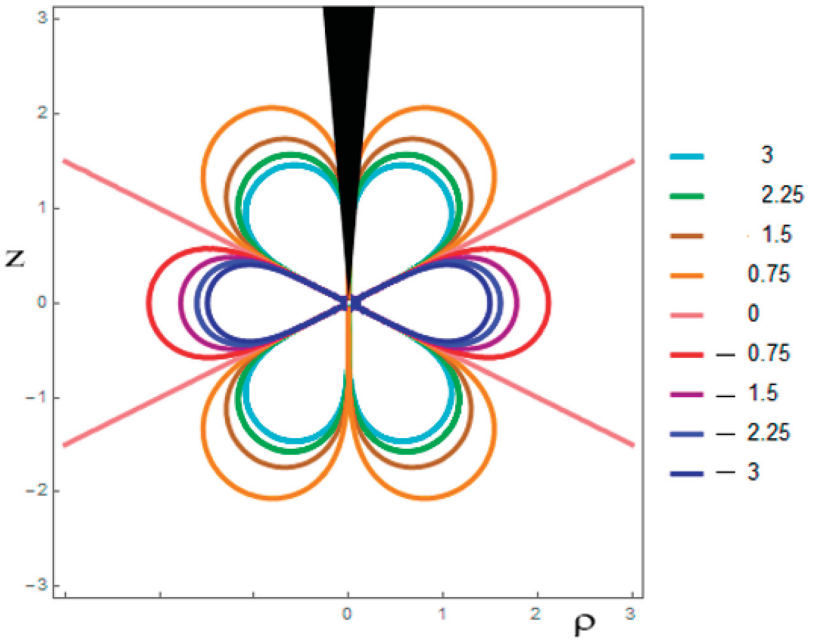

FIG. 3. Plot of azimuthal (toroidal) vorticity field following Eq. (47) (normalized with respect to $D\lambda_1\lambda_2 C_3$).

were conducted for a narrow homogeneous cone ($\alpha = 5^\circ$) and $\nu = 1$ (eigenvalue). Using the same parameters, a typical vorticity distribution [see Eq. (47)] is also depicted in Fig. 3 after normalization by $D\lambda_1\lambda_2 C_3$. As expected, a strong vorticity enhancement r^{-4} is observed near the rounded conical tip. Also note the sign change of the vorticity distribution within the sector $\theta = \pi/2 \pm \tan^{-1}(1/2)$. The different flow patterns between streamlines (Fig. 2) and azimuthal vorticity (Fig. 3) are connected with the fact that for the above chosen parameters, the numerically dominant term on the right-hand side of (43) is that proportional to C_1, whereas in Eq. (47) it is that corresponding to C_3.

V. SUMMARY AND DISCUSSION

Plasmofluidics is an emerging and promising field that combines plasmonics and nanofluids, which provides an efficient technological platform for manipulating nanoparticles and begetting indirect mixing in aqueous phases due to microvortices or nanovortices. Theoretical studies on plasmofluids are still scarce and here we have attempted to present an asymptotic analysis of the combined opto-electro-thermo effect, which can incite toroidal vortices in the solute near the tip of a coax metallic nanocone by means of localized (SPP) or converging (CPR) surface plasmonic resonances. A transverse-magnetic optical forcing by a low-input laser (e.g., helium-neon) operating in the visible to infrared frequency range was assumed and a solution for the Maxwell equations was presented in terms of conical and Bessel functions. We considered here a composite coaxial slender cone composed of two noble metals (for example, gold and silver) in perfect contact and derived a general dispersion relation for the surface plasmon polaritons propagating towards the tip in terms of the two dielectric coefficients and coax angles. We obtained a transcendental dispersion relation for the combined metacone, which degenerates into the corresponding known relation for a single homogeneous cone (where the permittivities of the two materials are equal).

By expressing the analytic eigensolutions for both magnetic- and electric-field components using the conical Mehler functions (Legendre polynomials of complex order $-1/2 + i\upsilon$) it was shown that the most singular (optimal) solution for the scattered electric field near the tip exhibits an r^{-3}-type singularity that corresponds to zero wave damping (no losses) and implies that the sought eigenvalue ν must be real. Furthermore, we showed that, in practice, a real eigenvalue cannot be attained under CPR conditions by a simple (homogeneous) metallic nanocone. One way of obtaining a real ν is by using a metamaterial coax cone composed of two separate noble metals with a perfect bond. We were able to analytically resolve the general transcendental dispersion relation under the assumption of a relatively small conical tapering angle and employing asymptotic expansions for the corresponding conical (Mehler) functions. An example was also provided for an optimal metamaterial (gold-silver) slender nanocone operating in the visible optical range with an opening angle of around 10° for which $\nu \sim 3$.

The large electric-field gradients induced near the rounded conical tip can be effectively used for sorting and controlling free NPs lying on a nearby substrate, which can experience a negative or positive DEP (i.e., moving towards or away from the cone axis), depending on the magnitude of the eigenvalue ν and sign of the CM coefficient. The electrokinetic response of a freely suspended NP is similar in many respects to that of the well-known trapping phenomena associated with optical tweezers. In addition to a controlled horizontal phoretic motion, the NP experiences also a vertical force that can be employed, for example, for levitation and sorting purposes of selected NPs. Adjustment of this modus operandi can be easily done by changing the distance of the substrate from the conical tip beyond a certain threshold value h^*.

It was finally demonstrated that plasmonic-induced dc nanovortices (mixing and pumping) can be induced in the aqueous phase even at relatively large optical frequencies. Fluid mixing is generated near the tip by the dielectric force density, which depends on the gradient (with respect to temperature) of the solute permittivity and the amplitude squared of the scattered electric field. The forcing gradient term arises from Joule heating effects in the conducting cone due to laser irradiation. By employing simple physical arguments, one can resolve the temperature distribution near the rounded tip of a narrow cone and analytically determine the stream function and velocity field near the tip from

the inhomogeneous Stokes equation. Using the same near-field methodology, it is also possible to obtain a rather simple expression for the induced dc azimuthal (toroidal) vorticity distribution in terms of the plasmonic eigenvalue ν. Thus, we have theoretically demonstrated a plasmofluidic or an opto-thermo-fluidic mechanism, by which fluid mixing due to steady (dc) nanovortices can be optically (ac) incited in the aqueous phase near the tip a slender coax nanoconical superconductor illuminated (optical range) by common low-input lasers (e.g., HeNe) operating at frequencies well beyond the Maxwell-Wagner limit.

ACKNOWLEDGMENTS

We acknowledge partial support from BSF Grant No. 2009371 and ISF Grant No. 1945/14 and useful discussions held with Dr. Y. Green.

[1] T. B. Jones, *Electromechanics of Particles* (Cambridge University Press, Cambridge, 1995).
[2] M. Born and E. Wolf, *Principles of Optics* (Cambridge University Press, Cambridge, 1999).
[3] H. Morgan and N. G. Green, *AC Electrokinetics: Colloids and Nanoparticles* (Research Studies, Philadelphia, 2003).
[4] K. Hirano, Y. Baba, Y. Matsuzawa, and A. Mizuno, Manipulation of a single coiled DNA molecules by laser clustering of microparticles, Appl. Phys. Lett. **80**, 515 (2002).
[5] G. V. Soni, F. M. Hameed, T. Roopa, and G. V. Shivashankar, Development of an optical tweezer combined with micromanipulation for DNA and protein nanobioscience, Current Sci. **83**, 1464 (2002).
[6] R. T. Dame, Single-molecule micromanipulation studies of DNA and architectural proteins, Biochem. Soc. Trans. **36**, 732 (2008).
[7] L. Novotny and B. Hecht, *Principles of Nano-Optics* (Cambridge University Press, Cambridge, 2006).
[8] A. Ashkin, Acceleration and Trapping of Particles by Radiation Pressure, Phys. Rev. Lett. **24**, 156 (1970).
[9] D. K. Gramotnev, Adiabatic nano-focusing of plasmons by sharp metallic grooves: Geometrical optical approach, J. Appl. Phys. **98**, 104302 (2005).
[10] F. De Angelis, G. Das, P. Candelaro *et al.*, Nanoscale chemical mapping using three-dimensional adiabatic compression of surface plasmon polaritons, Nat. Nanotechnol. **5**, 67 (2010).
[11] D. K. Gramotnev and S. I. Bozhevolnyi, Plasmonic beyond the diffraction limit, Nat. Photon. **4**, 83 (2010).
[12] A. Petrin, Nano focusing of surface plasmon polaritons by the tapered metallic plasmonic waveguide: Optical angle near the apex, J. Nanoelectron. Optoelectron. **5**, 55 (2010).
[13] D. K. Gramotnev and S. I. Bozhevolnyi, Nano-focusing of electromagnetic radiation, Nat. Photon. **8**, 13 (2014).
[14] H. Raether, *Surface Plasmons on Smooth and Rough Surfaces on Grantings* (Springer, New York, 1988).
[15] S. A. Maier, *Plasmonics: Fundamentals and Applications* (Springer, New York, 2007).
[16] V. Klimov, *Nanoplasmonics* (CRC, Boca Raton, 2014).
[17] P. B. Johnson and R. W. Christy, Optical constants of noble metals, Phys. Rev. B **6**, 4370 (1972).
[18] O. Schnitzer, Singular perturbation approach to localized surface-plasmon resonance: Nearly touching metal nanospheres, Phys. Rev. B **92**, 235428 (2015).
[19] A. Moussiaux, A. Ronveaux, and A. Lucas, Surface plasmon oscillations for different geometrical shapes, Can. J. Phys. **55**, 1423 (1977).
[20] A. J. Babadjanyan, N. L. Margaryan, and K. V. Nerkarayan, Super focusing of surface polaritons in the conical structure, J. Appl. Phys. **87**, 3785 (2000).
[21] M. Ideman, Confluent tip singularity of the electromagnetic field at the apex of a material cone, Wave Motion **38**, 251 (2003).
[22] M. I. Stockman, Nanofocusing of Optical Energy in Tapered Plasmonic Waveguides, Phys. Rev. Lett. **93**, 137404 (2004).
[23] R. Rupin, Effect of non-locality on nanofocusing of surface plasmon field intensity in a conical tip, Phys. Lett. A **340**, 299 (2005).

[24] A. Pessian and R. H. Ritchie, Curvature effects in surface plasmon dispersion and coupling, Phys. Rev. B **71**, 115425 (2005).
[25] K. Kurihara, A. Otomo, A. Syouj, J. Takahara, K. Suzuki, and S. Yokahama, Superfocusing modes of surface plasmonic polaritons in a conical geometry based on the quasi-separation of variables approach, J. Phys. A: Math. Theor. **40**, 12479 (2007).
[26] M. W. Vogel and R. Gramotnev, Adiabatic nano-focusing of plasmons by metallic tapered rods in the presence of dissipation, Phys. Lett. A **363**, 507 (2007).
[27] N. A. Isaa and R. Guckenberger, Optical nanofocusing on tapered metallic waveguides, Plasmonics **2**, 31 (2007).
[28] D. K. Gramotnev, M. W. Vogel, and M. I. Stockman, Optimized nanofocusing of plasmons by tapered metal rods, J. Appl. Phys. **104**, 034311 (2008).
[29] K. V. Nerkarayan, A. A. Hakhoumian, and A. E. Babayan, Terahertz surface plasmon-polariton superfocusing in coaxial cone semiconductor structures, Plasmonics **3**, 27 (2008).
[30] A. Yanai and U. Levy, Plasmonic focusing with a coaxial structure illuminated by radially polarized light, Opt. Express **17**, 924 (2009).
[31] M. W. Vogel and D. K. Gramotnev, Shape effects in a tapered metal rods during adiabatic nanofocusing of plasmonics, J. Appl. Phys. **107**, 044303 (2010).
[32] A. Rusina, M. Durach, K. A. Nelson, and M. I. Stockman, in *Plasmonics: Metallic Nanostructures and their Optical Properties VIII*, edited by M. I. Stockman, SPIE Proc. Vol. 77571 (SPIE, Bellingham, 2010).
[33] Y. Wang, F. Plouraboue, and H.-C. Chang, Broadband converging plasmon resonance of a conical nano tip, Opt. Express **21**, 6609 (2013).
[34] P. Domachuk, C. Grillet, V. Ta'eed *et al.*, Microfluidic interferometer, Appl. Phys. Lett. **86**, 024103 (2005).
[35] D. Psaltis and S. R. Quake, Developing optofluidic technology through the fusion of microfluidics and optics, Nature (London) **442**, 381 (2006).
[36] X. Mao, Z. Stratton, A. A. Nawaz *et al.*, Optofluidic tunable micro lens by manipulating the liquid meniscus using a flared microfluidic structure, Biomicrofluidics **4**, 043007 (2010).
[37] Y. Yang, A. Q. Liu, L. K. Chin *et al.*, Optofuidic waveguide as a transformation optic device to light wave bending and manipulations, Nat. Commun. **3**, 651 (2012).
[38] Y. Zhao, Z. Stratton, F. Guo *et al.*, Optofluidic imaging: Now and beyond, Lab Chip **13**, 17 (2013).
[39] M. Wang, C. Zhao, X. Miao *et al.*, Plasmonofluidics: Merging light and fluids at the micro-/nanoscale, Small **11**, 4423 (2015).
[40] A. Jonas and P. Zemanek, Light at work: The use of optical forces for particle manipulation, sorting and analysis, Electrophoresis **29**, 4813 (2008).
[41] S. Abalde-Cela, C. Abell, Alvarez-R. A. Puebla, and L. M. Liz-Marzan, Real time dual channel multiplex SERS ultra-detection, J. Phys. Chem. Lett. **5**, 73 (2014).
[42] G. Yossifon, I. Frankel, and T. Miloh, On electro-osmotic flows through microchannel junctions, Phys. Fluids **18**, 117108 (2006).
[43] X. Miao, B. K. Wilson, and L. Y. Lin, Localized surface plasmon assisted microfluidic mixing, J. Appl. Phys. Lett. **92**, 124108 (2008).
[44] Y. Eckstein, G. Yossifon, A. Seifert, and T. Miloh, Nonlinear electrokinetic phenomena around nearly insulated sharp tips in microflows, J. Colloid Interface Sci. **338**, 243 (2009).
[45] Y. Wang, X. Cheng, and H.-C. Chang, Celebrating singularities: Mathematics and chemical engineering, Am. Inst. Chem. Eng. J. **59**, 1830 (2013).
[46] L. Robin, *Fonctions Sphériques de Legendre et Fonctions Sphéroïdales* (Gauthier-Villars, Paris, 1959).
[47] E. W. Hobson, *The Theory of Spherical and Ellipsoidal Harmonics* (Chelsea, New York, 1965).
[48] M. Abramowitz and I. A. Stegun, *Handbook of Mathematical Functions* (Dover, New York, 1965).
[49] L. B. Felsen and N. Marcuvitz, *Radiation and Scattering of Waves* (Prentice-Hall, Englewood Cliffs, 1973).
[50] T. Miloh, Conical potential flow about bodies of revolution, Q. J. Mech. Appl. Math. **29**, 35 (1976).
[51] J. A. Stratton, *Electromagnetic Theory* (McGraw Hill, New York, 1941).
[52] Y. Kawata, C. Xu, and W. Deng, Feasibility of molecular-resolution fluorescence near-field microscopy using multi-photon absorption and field enhancement near a sharp tip, J. Appl. Phys. **85**, 1294 (1999).

[53] H. A. Stone, J. R. Lister, and M. P. Brenner, Drops with conical ends in electric and magnetic fields, Proc. R. Soc. London A **455**, 329 (1999).
[54] E. Demekhin, S. Polyanskikh, and A. Ramos, Taylor cones in a leaky dielectric liquid under an AC electric field, Phys. Rev. E **84**, 035301(R) (2011).
[55] E. D. Palik, *Handbook of Optical Constants of Solids* (Elsevier, Amsterdam, 1997).
[56] M. A. Ordal, L. L. Long, S. E. Bell, R. R. Bell, R. W. Bell, and C. A. Word, Optical properties of metals in the infrared and far-infrared, Appl. Opt. **22**, 1099 (1983).
[57] A. L. Yarin, E. Zussman, J. H. Wendorf, and A. Greiner, Material encapsulation and transport to core-shell micro/nanofibers, polymers and carbon nanotubes and micro/nanochannels, J. Mater. Chem. **17**, 2585 (2007).
[58] G. Mie, Beitrage zur optik truber medien speziell kolloidaler metallosungen, Ann. Phys. (Leipzig) **330**, 377 (1908).
[59] A. Ashkin, J. M. Dziedzic, J. E. Bjorkholm, and S. Chu, Observation of a single-beam gradient force optical trap for dielectric particles, Opt. Lett. **11**, 288 (1986).
[60] L. Novotny, R. X. Bian, and X. S. Xie, Theory of Nanometer Optical Tweezers, Phys. Rev. Lett. **79**, 645 (1997).
[61] G. Volpe, R. Quidant, G. Badenes, and D. Petrov, Surface Plasmon Radiation Forces, Phys. Rev. Lett. **96**, 238101 (2006).
[62] E. Feigenbaum and M. Orenstein, Nano plasmon polariton modes of a wedge cross section metal waveguide, Opt. Express **14**, 8779 (2006).
[63] M. Righini, P. Ghenuche, S. Cherukulappurath, V. Myroshnychenko, F. J. García de Abajo, and R. Quidant, Nano-optical trapping of Rayleigh particles and *Escherichia coli* bacteria with resonant optical antennas, Nano Lett. **9**, 3387 (2009).
[64] M. L. Juan, M. Righini, and R. Quidant, Plasmon nano-optical tweezers, Nat. Photon. **5**, 349 (2011).
[65] Y. Li, L. Xu, and B. Li, Gold nanorod-induced localized surface plasmon for microparticle aggregation, Appl. Phys. Lett. **101**, 053118 (2012).
[66] R. Kotb, M. E. Maklizi, Y. Ismail, and M. A. Swillam, Optical trapping and manipulations of nanoparticles using meta plasmonic structure, J. Opt. **18**, 015002 (2015).
[67] M. I. Petrov, S. V. Sukhov, A. B. Bogdanov, A. S. Shalin, and A. Dogariu, Surface plasmon polaritons assisted optical pulling force, Laser Photon. Rev. **10**, 116 (2016).
[68] T. M. Squires and M. Z. Bazant, Induced-charge electro-osmosis, J. Fluid Mech. **509**, 217 (2004).
[69] A. Ramos, H. Morgan, N. G. Green, and A. Castellanos, AC electrokinetics: A review of forces in microelectrodes structures, J. Phys. D **31**, 2338 (1998).
[70] H. Green, A. Ramos, and N. G. Green, AC electrokinetics: A survey of sub-micrometer particle dynamics, J. Phys. D **33**, 632 (2000).
[71] G. Baffou, R. Quidant, and C. Girard, Heat generation in plasmonic nanostructures: Influence of morphology, App. Phys. Lett. **94**, 153109 (2009).
[72] G. Baffou, R. Quidant, and F. J. García de Abajo, Nanoscale control of optimal heating in complex plasmonic systems, ACS Nano **4**, 709 (2010).
[73] J. S. Donner, G. Baffou, D. McCloskey, and R. Quidant, Plasmon-assisted optofluidics, ACS Nano **5**, 5457 (2011).
[74] G. Baffou and R. Quidant, Thermo-plasmonics: Using metallic nanostructures as nano sources of heat, Laser Photon. Rev. **7**, 171 (2013).
[75] O. Blum and N. T. Shaked, Prediction of photo-thermal phase signatures from arbitrary plasmonic nanoparticles and experimental verification, Nat. Light: Sci. Appl. **4**, 1038 (2015).
[76] M. Enders, S. Mukai, T. Uwada, and S. Hashimoto, Plasmonic nanofabrication through optical heating, J. Phys. Chem. C **120**, 6723 (2016).
[77] S. Berwerger, J. M. Atkin, R. L. Olmon, and M. B. Raschke, Light on the tip of a needle: Plasmonic nanofocusing for spectroscopy on a nanoscale, Phys. Chem. Lett. **3**, 945 (2012).
[78] C. Huber, A. Trugler, U. Hohenester, Y. Prior, and W. Kautek, Optical near-field excitation at commercial scanning probe microscopy tips: A theoretical and experimental investigation, Phys. Chem. Chem. Phys. **16**, 2289 (2014).

[79] P. I. Geshev, S. Klein, and K. Dickmann, Calculations of the temperature and thermal expansion of a STM tip heated by a short laser pulse, Appl. Phys. B **76**, 313 (2003).
[80] M. Stahelin, M. A. Bopp, A. Tarrach, A. J. Meixner, and I. Zschokko-Granacher, Temperature profile of fiber tip used in scanning near field optical microscopy, Appl. Phys. Lett. **68**, 2603 (1996).
[81] P. Solana, P. Kapadia, and J. Dowden, A mathematical analysis of heating effect and electrode erosion in conical electrical arc cathodes, J. Phys. D **31**, 3446 (1998).
[82] R. Kodoma, H. Azechi, H. Fujita *et al.*, Fast plasmon heating in a cone-attached geometry toward fusion ignition, Nucl. Fusion **44**, 5276 (2004).
[83] X. Chen and X. Wang, Near-field thermal transport in a nanotip under laser radiation, Nanotechnology **22**, 075204 (2011).
[84] J. Mihaljevic, S. Slama, R. Ropke, and A. J. Meixner, Geometric tailoring of plasmonic nanotips for atom traps, Phys. Rev. A **90**, 013421 (2014).
[85] A. O. Govorov and H. H. Richardson, Generating heat with metal nanoparticles, Nano Today **2**, 31 (2007).
[86] H. H. Richardson, M. T. Carlson, P. J. Tandler *et al.*, Experimental and theoretical studies of light-to-heat conversion and collective heating effects in metal nanoparticle solution, Nano Lett. **9**, 1139 (2009).
[87] B. J. Roxworthy, A. M. Bhuiya, S. P. Vanka, and K. C. Toussaint, Jr., Understanding and controlling plasmon-induced convection, Nat. Commun. **5**, 3173 (2014).
[88] J. M. Crowley, Role of Joule heating in the electrostatic spraying of liquids, J. Appl. Phys. **48**, 145 (1977).
[89] M. N. Ozisik, *Heat Transfer: A Basic Approach* (McGraw-Hill, New York, 1985).
[90] R. Muki and E. Sterenberg, Steady-state heat conduction in a circular cone, Z. Angew. Math. Phys. **9**, 306 (1960).
[91] M. Pichaud, A. Muller, and M. Drechsler, Temperature distribution along metal tips, Surf. Sci. **26**, 14 (1971).
[92] V. Gerester, A. Thon, and W. Pfeiffer, Thermal effects in pulsed laser assisted scanning tunneling microscopy, J. Appl. Phys. **87**, 2574 (2000).
[93] J. Happel and H. Brenner, *Low Reynolds-Number Hydrodynamics* (Nijhof, The Hague, 1983).
[94] E. Yariv and T. Miloh, Electro-convection about conducting particles, J. Fluid Mech. **595**, 163 (2008).
[95] A. Mizuno, M. Nishioka, Y. Ohno, and L. D. Dascalescu, Liquid micro vortices generated around a laser focal point in an intense high frequency electric field, IEEE. Ind. Appl. **31**, 464 (1995).
[96] A. Kumar, S. J. Williams, and S. T. Wereley, Experiments on opto-electrically generated microfluidic vortices, Microfluid. Nanofluid. **6**, 637 (2007).
[97] C. Park and S. T. Wereley, Rapid generation and manipulation of microfluidic vortex flow induced by AC electrokinetics with optical illumination, Lab Chip **13**, 1280 (2013).
[98] R. C. Ackerberg, The viscous incompressible flow inside a cone, J. Fluid Mech. **21**, 47 (1965).
[99] E. W. Schwiderski, H. J. Lugt, and P. Ugincius, Axisymmetric viscous fluid motion around conical surfaces, J. SIAM Appl. Math. **14**, 191 (1966).